Salt-dependent properties of a coacervate-like, self-assembled DNA liquid

SCHOLARONE™
Manuscripts

Soft Matter

ARTICLE TYPE

Salt-dependent properties of a coacervate-like, self-assembled DNA liquid[†]

Byoung-jin Jeon,[a] Dan T. Nguyen,[b] Gabrielle R. Abraham,[c] Nathaniel Conrad,[c] Deborah K. Fygenson,[b,c] and Omar A. Saleh*[a,b]

Liquid-liquid phase separation of a polymer-rich phase from a polymer-dilute solution, known generally as coacervation, has been observed in a variety of biomolecular systems. Understanding of this process, and the properties of the resulting liquid, has been hampered in typical systems by the complexity of the components and of the intermolecular interactions. Here, we examine a single-component system comprised entirely of DNA, in which tetravalent DNA nanostar particles condense into liquids through attractive bonds formed from basepairing interactions. We measure the density, viscosity, particle self-diffusion, and surface tension of NS-liquid droplets. The sequence- and salt-dependent thermodynamics of basepairing accounts for most properties, particularly indicating that particle transport is an activated process whose barrier is the breaking of a single bond, and that very few bonds are broken at the surface. However, more complex effects are also seen. The relation of density to salt shows that electrostatic screening compacts the NS particles. Further, the interrelation of the transport properties indicates a breakdown of the Stokes-Einstein relation. This observation, in concert with the low surface tension and single-bond transport barrier, suggests this DNA liquid has a heterogeneous, clustered structure that is likely enabled by internal NS particle flexibility. We discuss these results in comparison to other coacervate systems.

Certain biomolecular solutions have the ability to undergo liquid-liquid phase separation (LLPS), forming dense liquid droplets in equilibrium with a dilute biomolecular 'gas'. Phase separation is frequently driven by electrostatic attraction between oppositely charged biopolymers, a process termed complex coacervation. This process has been the subject of intense study, partially because of the variety of potential applications (e.g. drug delivery, food processing, and cosmetics).[1–4] More recently, electrostatically-driven biomolecular LLPS has been identified in biological contexts, where the resulting droplets form within cells, creating biochemically-distinct spaces that are typically termed 'membrane-less organelles'.[5,6]

[a] Materials Department, University of California, Santa Barbara, Santa Barbara, CA 93106, USA.

[b] Biomolecular Science and Engineering Program, University of California, Santa Barbara, Santa Barbara, CA 93106, USA.

[c] Physics Department, University of California, Santa Barbara, Santa Barbara, CA 93106, USA.

* E-mail: saleh@ucsb.edu

Mutually attractive macromolecular particles can form a variety of condensed structures, such as crystals, gels, or liquids. It has been suggested that liquids will outcompete other phases when the component particles have internal flexibility, and when the interacting particles are of limited valence (i.e. when each particle has only a few attractive patches where particle-particle bonds can form).[5,7] A major advance was the realization that such parameters could be designed into multi-armed, self-assembled DNA nanoparticles, termed nanostars (NSs).[8] NSs exhibit internal flexibility due to the presence of relatively floppy, unpaired bases at key locations, and achieve a limited valence by designing attractive hybridization interactions to only occur at the tips of the arms. Simulations showed how these features lead to the stability of the NS-liquid with respect to the crystalline phase.[9] Experimental studies demonstrated equilibrium LLPS in the NS system,[8] and illuminated the role of unpaired bases in permitting particle mobility within the condensed phase, which is key to avoiding kinetic trapping of NSs in a gel structure.[10]

Typical coacervate systems involve either multiple components, a wide range of molecular configurations, a variety of types of intermolecular interactions, and combinations thereof. This complexity has hindered both understanding of microscopic coacervate structure, and examination of coacervate properties. In
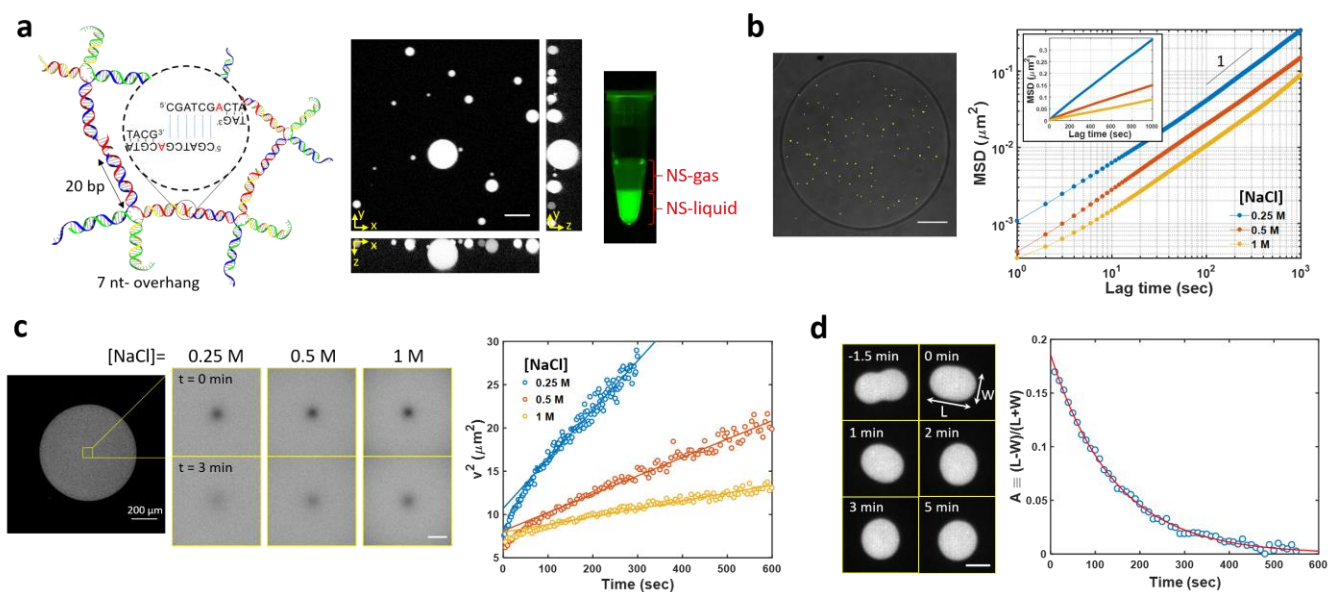
Fig. 1 (a) Left: Schematic of individual NS constructs comprised of four ssDNA oligos (each strand is a distinct color) and of the formation of a NS-liquid via DNA hybridization between NS overhangs. Center: Confocal image of phase separated NS droplets at 0.5 M NaCl. A mixture of untagged and Cy3-tagged NSs (99:1) was used for fluorescent visualization at 561 nm excitation. XZ(right) and YZ(bottom) projections show the spherical shape of the droplets (scale bar, 20 μm). Right: Bulk phase separation of ~100 μL of NS solution. NSs are visualized by adding YOYO-1 at 1:100 dye:NS molar ratio. (b) Left: Confocal image of fluorescent probe particles (yellow) embedded in a large NS droplet (scale bar, 20 μm). Right: Log-log plots of averaged mean squared displacement (MSD) of the probe particles at three different concentrations of NaCl. (inset) Linear-linear plot. (c) Left: Representative images of FRAP within NS droplets taken right after (i.e. postbleach) and 3 min after bleaching at [NaCl]=0.25, 0.5, and 1 M (scale bar, 10 μm). Right: v^2 vs. time, where v^2 is the variance of the Gaussian function of the radial intensity profile, fits to a straight line at long time scales with slope $2D$ at each [NaCl], where D is a diffusion coefficient. (d) Left: Coalescence event of two NS-liquid droplets imaged over time (scale bar, 5 μm). Right: Aspect ratio of a NS-liquid is defined as $A \equiv (L-W)/(L+W)$ where L and W are the length and width of the deformed droplet under relaxation. All experiments were carried out at 20 °C.

contrast, the DNA NS system involves only a single type of self-attractive particle, and has interactions dominated by well-characterized basepairing interactions; thus, we suggest the NS system can serve as a useful model for LLPS properties and behavior. To that end, we here carry out a rigorous investigation of the salt-dependent density, viscosity, self-diffusivity, and surface tension of a NS-liquid. These parameters exhibit a contrary response to salt compared to typical coacervates, due to the dominant role played by salt-induced electrostatic screening in DNA hybridization. Indeed, quantitative modeling shows that hybridization thermodynamics can explain many of the measured properties. Yet, effects beyond hybridization are needed to explain the measured variation in density, the low surface tension, and the observed breakdown of the Stokes-Einstein relation. Altogether, our data implies that the NS-liquid has a heterogenous, clustered structure. More broadly, NS-liquids exhibit low densities, high viscosities, and anomalous structural properties; these distinct qualities have implications for other macromolecular LLPS systems, as well as indicating the potential of the NS system as a substrate for biomolecular engineering.

1 Results

DNA NSs were assembled from four distinct single-stranded DNA (ssDNA) oligos, as described previously. [8,10] The oligos hybridize to create a structure with four 20 bp arms that meet at a junction, where the arms are separated by two unpaired adenosine bases. Distal from the junction, each double-stranded DNA (dsDNA) arm terminates in the same seven nucleotide (nt) ssDNA 5' tail with sequence 5'−$CGATCGA$−3'. The palindromic $CGATCG$ portion of this tail constitutes a sticky-end that permits NS-NS binding, while the 3' A is left unpaired (Fig. 1a).

The NS-liquid phase is expected to be salt-sensitive, due to charge screening effects on the repulsion between negatively-charged phosphate groups. Screening affects sticky-end hybridization as well as the electrostatic repulsion between NSs and between arms within a single NS. To investigate this, we first examined how changes in salt concentration affect the density of DNA within the NS-liquid. With sufficient salt, and at low temperatures, NSs interact to form DNA-rich, spherical NS-liquid droplets within a DNA-dilute aqueous 'NS-gas' (Fig. 1a). The two phases can be separated using centrifugation and extracted for analysis with absorbance spectroscopy. As expected for a phase equilibrium, the DNA concentration in the NS-liquid phase is independent of the overall NS concentration(Fig. S1). The DNA concentration of the NS-liquid phase increases from 19.2 (±1.8) to 35.1 (±1.1) mg/mL at 20 °C, corresponding to DNA volume fractions φ = 0.011 to 0.021, as [NaCl] increases from 0.25 to 1 M (Table 1). Alternate density estimates, based on sedimentation velocities of isolated droplets(Fig. S2), are consistent with these concentrations, indicating that neither the centrifugation process nor the transformation of NS-liquid droplets into a bulk phase affects NS-liquid density.

We measured the viscosity of NS-liquids at various [NaCl] via microrheology (Fig. 1b) and found results that match estimates from bulk rheology(Fig. S3). Microrheology was performed by embedding fluorescent probe particles (200 nm diameter) into large NS droplets (diameter >50 μm) and tracking their mean squared displacement (MSD) over time at 20 °C. NS-liquids exhibit viscous behavior at long time scales, with a diffusive exponent α, from $(MSD) \sim \tau^\alpha$ with lag time τ, that is near-unity at all measured [NaCl] (Fig. 1b). We note that, at short time scales, α deviates slightly from unity. This might be due to the onset of an elastic response, as observed in bulk rheology measurements(Fig. S3), or it might be a consequence of displacements at short time scales being of similar magnitude to particle-tracking noise [11,12]. Regardless, our focus here is on the well-resolved long-time dynamics. Diffusivity of the probe particles in the NS-liquid, D_{probe}, was obtained by fitting the long time data (τ > 100 sec) to $(MSD) = 4D_{probe}\tau^\alpha$, where the factor of four is used because the particles are tracked in two dimensions. Viscosity η of the NS-liquid, computed from the Stokes-Einstein relation, increases with ionic strength, changing more than 3 fold, from 24 to 90 Pa·sec, as [NaCl] increases from 0.25 to 1 M (Table 1).

The internal dynamics of NS-liquids (i.e. the mobility of individual NSs) can be probed using fluorescence recovery after photobleaching (FRAP). To achieve this, one of the component NS oligos was modified to include an internal Cy3 dye. Mixtures of 99:1 untagged:Cy3-tagged NSs were used to form fluorescent NS-liquid droplets. Using confocal microscopy, a point in the center of each droplet was bleached and the fluorescence recovery was subsequently tracked. Time scales of recovery were extracted from the time-dependent variance v^2 of the Gaussian function describing the intensity profile of a bleached spot(Fig. S4). For each [NaCl], we observe a fast response within the initial seconds of recovery followed by a slow relaxation (Fig. 1c). The origin of the fast recovery is unclear; it might be due to diffusion of free (unbound) DNA NS, or a consequence of photodamage that occurs during the bleaching step. We focus on the slow recovery (t >60 sec) where v^2 grows linearly with time, consistent with expectations for diffusion. [13] Since the slope of that linear dependence is 2D, we can use it to calculate diffusion coefficients D; we find that D significantly decreases as [NaCl] increases (Table 1).

The properties of any liquid/gas interface are defined by the surface tension, which here is again expected to be salt-dependent for NS-liquid droplets. To quantify this, we exploit the frequent observation of coalescence events, in which two or more NS droplets collide and merge (Fig. 1d). Experiments were done with droplets collected on a surfactant-coated oil-water interface so as to minimize the effects on coalescence dynamics from adhesion to, or excess drag from, external surfaces. At late stages, coalescing droplets form ellipsoids that relax to spheres over a characteristic time τ that varies with final droplet radius R and surface tension σ. [14] In the present case, where the internal (i.e. NS-liquid) viscosity η_{int} is much larger than the external (i.e. NS-gas) viscosity, the relation is

$$\tau \cong \frac{19 \, \eta_{int} R}{20 \, \sigma} \tag{1}$$

Using τ from exponential fitting to the trajectory of the droplet aspect ratio and η_{int} from microrheology, we find that as [NaCl] increases, surface tension also increases (Table 1).

Table 1 Physical properties of NS-liquids: DNA concentration (c_{DNA}), viscosity (η), self-diffusion coefficient (D), and surface tension (σ)

[NaCl] (M)	c_{DNA} (mg/mL)	η (Pa·sec)	D (10^{-3} μm^2/sec)	σ (μN/m)	$D\eta$ (Pa·μm^2)
0.25	19.2 ± 1.8	24 ± 4	27 ± 5	1.23 ± 0.06	0.65
0.5	24.9 ± 0.3	45 ± 3	9 ± 3	2.28 ± 0.13	0.41
1	35.1 ± 1.1	88 ± 17	3.6 ± 0.9	3.7 ± 0.4	0.32

2 Discussion

2.1 Role of DNA basepairing thermodynamics

Since the NS-liquid condenses through DNA hybridization of the overhangs, we expect a major mechanism of salt modulation of liquid properties will be through its effects on DNA hybridization. Indeed, this is qualitatively observed in most of the properties measured (see Table 1): higher [NaCl] leads to more stable bonds, which increases the dissipation upon flow (increasing the viscosity) and keeps each NS bound longer to its neighbors (decreasing the diffusivity). Further, stronger binding increases the preference for NS-NS interactions over interactions with the solvent, thereby increasing the surface tension. An estimate for such effects can be made by calculating the salt-dependent hybridization probability of the overhangs using existing DNA thermodynamics databases, and by ignoring connectivity of overhangs within a NS (see Supporting material); this gives upper bounds of the hybridization probability of 98.7, 99.2, and 99.5%, per overhang, for 0.25, 0.5, and 1 M salt, respectively. This rough estimate does clarify the relatively strong nature of the bonding in the system; however, as it shows very high and practically unchanging values with [NaCl], it does not help explain the relatively strong dependence with salt of our results.

Quantitative analysis of the free energy of overhang hybridization, rather than the binding probability, better illuminates the role of salt-dependent hybridization in determining D, η, and σ. SantaLucia has shown that the free energy of DNA duplex formation can be estimated, in units of kcal/mol, as $\Delta G = -(3.68 \times 10^{-4})NT \ln [\text{salt}] + C$, where N is half the number of phosphates in the duplex, T is temperature in K, [salt] is the monovalent salt concentration in molar, and the constant $C \approx -9.5$ kcal/mol is the hybridization free energy at 1 M salt and $T = 293$ K for the particular sequence design used here. [15] We expect the surface tension to be sensitive to unbound NS arms at the liquid surface; thus, we expect $\sigma \propto |\Delta G|/v_{mol}^{2/3}$, where v_{mol} is the volume occupied by one molecule of NS in the NS-liquid phase. The denominator tracks the area per molecule on the surface and assumes the available space per molecule is the same on the surface as in the bulk. We thus expect $\sigma v_{mol}^{2/3} \propto \ln [\text{NaCl}]$, which is confirmed by the data (Fig. 2c). v_{mol} was calculated via $v_{mol} = MW_{NS}/(c_{DNA} \cdot N_A)$, where MW_{NS} is the molecular weight of a NS and N_A is Avogadro's number. The values of v_{mol} used here are 5190, 4000, and 2840 nm^3 for [NaCl] = 0.25, 0.5, and 1 M, respectively.

Interestingly, the absolute values of $\sigma v_{mol}^{2/3}$ are 100-fold below the energy of a single bond, e.g. at 1 M salt, $\sigma v_{mol}^{2/3} \approx 4 \times 10^{-22}$ J, while $|\Delta G| \approx 9$ kcal/mol $\approx 6 \times 10^{-20}$ J. We posit this can be explained by a structure in which the majority of the NSs on the surface retain the same number of bonds as NSs in the bulk, with internal flexibility permitting these surface NSs to orient all arms inwards. The surface tension could then be attributed to bonds lost (relative to bulk) by a minority of surface NSs. A more complex picture is needed to account for the effect of reorientation of NSs at the surface, which will create a surface-excess entropy that would also contribute to σ. Regardless, while the scaling with salt demonstrates that σ is controlled by overhang bonding, the 100-fold factor between $\sigma v_{mol}^{2/3}$ and $|\Delta G|$ indicates that there are relatively few unbound arms at the surface.

We relate the transport properties, η and D, to ΔG by positing that transport within the liquid is an activated process, in which a NS breaks bonds with its neighbors, moves, then rebonds in a new position. The activation energy of this process, E_a, will thus be given by the free energy, ΔG, of the bonds, and the number, m, of bonds broken: $E_a = m|\Delta G|$. The time scale, τ, of transport should then follow Arrhenius behavior, $\tau \sim \exp(E_a/RT)$, where R is the gas constant. Using the experimental conditions ($N = 5$, $T = 293$ K), this gives a power-law dependence, $\tau \sim [\text{salt}]^{0.93m}$. We expect this time scale controls both viscosity and diffusivity: $\eta \propto \tau$, $1/D \propto \tau$. The experimental data both show near-linear dependencies: $\eta \propto [\text{salt}]$, $1/D \propto [\text{salt}]$ (Fig. 2a & b). This generally indicates that hybridization thermodynamics account for the transport properties, and specifically indicates that $m \approx 1$, i.e. that the basic process limiting transport is the breaking of a single NS-NS bond. Although η and D are expected to have a prefactor that depends on density, [16] that effect is minor compared to the salt dependence. Finally, we note these results are fully-consistent with the results of Bomboi *et al.*, [17] who observed ln [salt] dependency of the free energy barrier associated with NS dynamics.

Overall, the results in Fig. 2 imply that all three NS-liquid physical properties explored in this study are dominated by NS-NS overhang hybridization. This is confirmed using NSs with a stronger overhang sequence (i.e. larger $|\Delta G|$), which indeed exhibits a higher viscosity (Fig. S5), confirming the potential of sequence-dependent control of NS-liquid properties.

2.2 Beyond basepairing: Density, Stokes-Einstein behavior, and clustering

Interestingly, certain aspects of our data cannot be attributed to effects of salt-dependent hybridization. This includes the effect of salt on NS-liquid density, c_{DNA}. Qualitatively, salt-induced bond stabilization should lead to more neighbors per NS, and an increase of density with salt, as observed. Quantitatively, one might expect this trend to saturate when the number of neighbors approaches four (i.e. the NS valence) at a value near the density of NSs in a diamond lattice, here corresponding to $c_{DNA} \approx 13.3$ mg/mL. [8] However, we measure droplet densities that far surpass
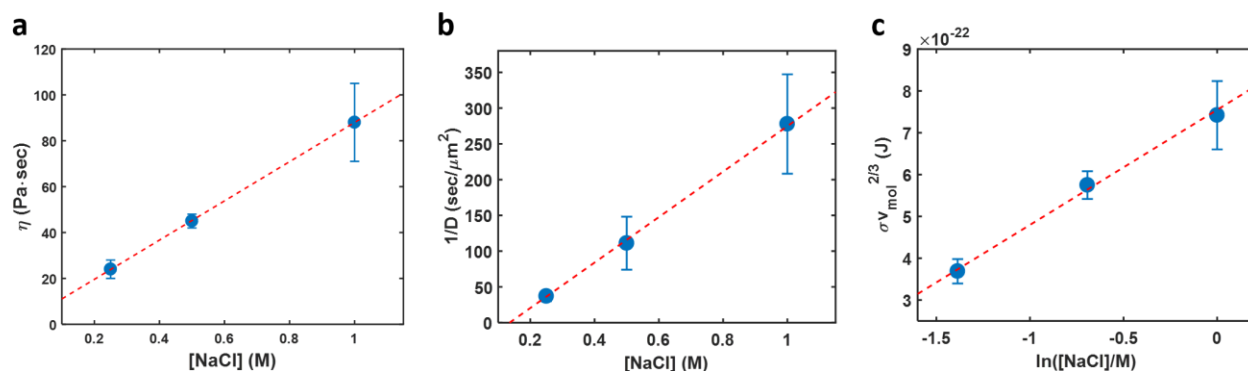
Fig. 2 The relationships of (a) viscosity, (b) diffusivity, and (c) surface tension with [NaCl] indicate each parameter is sensitive to the energetics of DNA hybridization.

this estimate. We speculate that high salt concentrations alter NS-liquid structure and enhance NS-liquid density not just by saturating NS bonds, but by screening electrostatic repulsion between NSs, or even within a NS. The latter would permit closer approach of NS arms, or base-stacking across the NS junction; such effects are seen in Holliday junctions, 4-armed DNA structures of biological significance. [18,19]

Simple hybridization arguments also fail to explain the relation of the measured transport properties, D and η. In the NS-liquid phase, both diffusive transport and shear flow are hindered by NS-NS binding; thus, it is reasonable to expect that D and η will vary in a correlated fashion as binding interactions are perturbed by changes in salt. A standard prediction for this correlation is the Stokes-Einstein relation, which predicts that the product $D\eta$ is a constant, so long as the temperature and the particle size do not vary. [20,21] Here, however, we find that $D\eta$ is sensitive to salt (Table 1), showing a strong decrease as [NaCl] increases. This might be attributed to a salt-dependent change in particle size, but the trend is opposite of what is expected. Our density measurements indicate the available volume per particle, v_{mol}, decreases with salt; further, intra-NS screening effects would lead to a smaller size of NSs at higher salts. If such salt-dependent compaction were the only effect, $D\eta$ would increase with salt, in contrast to what is observed. The strong decrease in $D\eta$ is likely due to the increased importance of collective effects at high salt concentrations: as bond strength increases at higher salt, NSs form larger and more stable effective clusters within the liquid, which diffuse progressively more slowly. Such collective dynamic behaviors are a characteristic feature of liquids with network structures similar to the present NS system, [22,23] lending support to this interpretation.

The existence of stably-bonded clusters of NS is somewhat at odds with the observation that transport is controlled by a single-bond activation barrier (i.e. $m \approx 1$): The former implies a relatively integrated structure, with each NS participating in multiple bonds, yet the latter suggests that breaking only a single bond enables NS mobility. We speculate that this can be reconciled by the existence of a heterogenous structure in the liquid, in which NSs are indeed well-bonded to neighbors within the same cluster, but with relatively few bonds connecting neighboring clusters, such

that breaking of a single cluster-cluster bond induces mobility. This would indicate that most NSs at a cluster-cluster interface orient their bonds inwards (into their cluster), rather than across the interface; this is consistent with our interpretation of the magnitude of the surface tension, as discussed above.

2.3 Conclusion and comparison to other coacervate systems

The unique features of NS-liquids become clear when compared to those of other reported biomolecular liquids, such as synthetic coacervates and liquids derived from components of intracellular droplets (see Table 2). The most salient difference is that NS-liquid properties respond to salt in the opposite manner as the other systems. This occurs because the NS-liquids form due to salt-stabilized DNA hybridization, while the other systems form due to electrostatic attractions, which are weakened by added salt.

Table 2 also points out that the various biomolecular liquids vary strongly regarding their density; note that the variation in the remaining properties (viscosity and surface tension) can roughly be understood as being sensitive to density. Synthetic coacervate systems are generally at least 10-fold more dense than the other systems, likely because the constituent polymers tend to be highly-charged and flexible, permitting each chain to contact many oppositely-charged chains, thus driving higher liquid densities. [25] In contrast, the present NS-liquid system has a limited valence: strong interparticle contact is permitted only at the four overhangs, which decreases particle packing and liquid density. Further, we expect that the stiff nature of the DNA arms contributes to the low density by pushing bound particles away from each other. Interestingly, single-component liquids formed from purified LAF1, a protein derived from an intracellular droplet system, achieve an extraordinarily low density ($\varphi \approx 0.3\%$). The researchers attributed the expansive occupied volume in their system to large configurational fluctuations of the protein. [34]

Brangwynne and colleagues have suggested that the low density of intracellular droplets may have evolved to accommodate the free diffusion of small molecules within the meshwork of the macromolecular liquid, thereby allowing biochemical reactions to occur. [34] We suggest that NS-liquids could similarly permit chemical activation through the action of permeable species, perhaps

Table 2 Physical properties of various coacervate and biomolecular liquid systems (response to increasing [salt])

System	Fraction macromolecule	Viscosity (Pa·sec)	Surface tension (N/m)	Ref.
DNA NS droplets	2–3.5 wt% $\varphi \approx 0.01$–0.02 (increase)	10^1 (increase)	10^{-6} (increase)	this study
Synthetic coacervates (Polyelectrolytes/polypeptides/ polysaccharides)	15–35 wt% $\varphi \approx 0.1$–0.4 (decrease)	10^1–10^5 (decrease)	10^{-5}–10^{-4} (decrease)	24–30
Intracellular droplets	0.3–0.8 wt% $\varphi \approx 0.002$–0.006 (decrease)	10^0–10^1 (decrease)	10^{-6}–10^{-4} (decrease)	12,31–34

permitting the DNA system to act as an *in vitro* model for testing the biological implications of sparse liquid structure. In this context, the ability to tune NS structure through sequence is a potent feature that enables control of liquid physical characteristics in varied solution conditions.

3 Methods

3.1 DNA Nanostars

DNA NS were annealed as previously described. [8] Briefly, four DNA sequences, [10] synthesized and desalted by Integrated DNA technologies, were mixed in equimolar concentrations in 10 mM Tris-HCl (pH 7.5), incubated at 95 °C for 5 min, and cooled to 4 °C at -0.5 °C/min. The annealing procedure was validated to produce > 90% correctly formed NS, confirmed through observation of a single dominant band in gel electrophoresis, as described previously. [8,10] When fluorescent visualization is necessary, one of the DNA oligos was replaced with a variant containing an internal Cy3 dye at the 3' end of the overhang. Cy3-tagged NSs were diluted 100-fold with untagged NSs for use in all experiments requiring fluorescence. Cy3-tagged NSs integrate homogeneously into NS-liquids (Fig. 1).

3.2 Density and volume fraction

100 μL solutions of 5–15 mg/mL DNA NS were prepared with 0.25, 0.5, or 1 M NaCl, with 1:100 molar ratio of YOYO-1:NS. The NS solutions were incubated at 50 °C for 30 min and centrifuged at 3,000 x g for 100 min. Using a transilluminator (Invitrogen) for visualization (Fig. 1a), the DNA-dilute phase was removed via pipette. The DNA concentration of the resulting NS-liquid was then measured via absorbance at 260 nm using a Nanodrop One spectrophotometer (Thermo Fisher Scientific). Volume fraction was calculated as $\varphi = c_{DNA}/(1.7 \text{ g/cm}^3)$. [35]

3.3 Microrheology

Mixtures of NS and 200 nm fluorescent beads (540 ex/560 em, FluoSpheres[TM] from Thermo Fisher Scientific) were added into 10 μL of tris buffer at [NaCl] of 0.25, 0.5, and 1 M and incubated overnight at room temperature on a rotator, thereby allowing formation of large (> 50 μm) spherical NS droplets. NS-liquid droplets were introduced into a flowcell (i.e. a coverslip-parafilm-coverslip sandwich with a channel cut in the parafilm) using end-cut pipette tips, and subsequently sealed with epoxy. The mobility of fluorescent beads in NS-liquids were tracked with confocal

microscopy for > 100 min with 1 sec intervals. MSDs were calculated and fit to the form $MSD(\tau) \sim 4D_{probe}\tau^\alpha$, where α is the diffusive exponent, to estimate the diffusion coefficient D_{probe}. Viscosities η of DNA NS-liquids at different [NaCl] were then calculated using the Stokes-Einstein equation, $D_{probe} = k_B T /6\pi\eta r$, where k_B is the Boltzmann constant, $T = 293$ K is temperature, and $r = 100$ nm is the probe radius.

3.4 Fluorescence Recovery After Photobleaching

Fluorescent NS-liquid droplets, containing a 99:1 mixture of untagged:Cy3-tagged NSs, were imaged using a Leica SP8 confocal microscope. Image acquisition and data analysis was carried out following the method described by Seiffert and Oppermann. [13] Briefly, samples were imaged (512 x 512 pixels) using an objective with low numerical aperture (10x; 0.3 NA) with 20x zoom. A point was bleached with 550 nm excitation (10 sec at 50% laser power, which was measured to be about 0.5 mW at the sample level) and fluorescent recovery was examined over $558 - 717$ nm emission at 2, 5, and 5 sec intervals for 0.25, 0.5, and 1 M [NaCl], respectively. The average fluorescent intensity, $I(r)$, at a given radius from the bleached spot, r, was calculated at each recovery time point and fit to the equation $I(t, r) = I_0(t) - A(t) \exp(-r^2/2v(t)^2)$, where v^2 is the time-dependent variance of the Gaussian function(Fig. S4).

3.5 Coalescence experiments

Coalescence was observed for fluorescent NS-liquid droplets on a flat oil/water interface. [36] Briefly, a flow cell was prepared where the surface of the bottom coverslip was made hydrophobic with Sigmacote[S] (Sigma-Aldrich). 2% of PFPE-PEG-PFPE Tri-block-copolymer Surfactant (E2K0660; RAN Biotechnologies, Inc.) in 3M[TM] Novec[TM] 7500 Engineered Fluid (3M) was prepared and wicked into the flow cell. Then, an aqueous solution of pre-formed NS-liquid droplets in the salt of interest was flowed into the flow cell. The result is a flat oil/water interface where individual NS-liquid droplets can diffuse laterally, with minimal friction, to encounter and coalesce with other droplets. Coalescence events were recorded with confocal microscopy (Visitech), where 3D volumes were captured with 10 sec intervals at 561 nm excitation.

To calculate surface tensions, we use a formulation by Leal that shows, at late stages, the relaxation timescale τ of the transformation of an elliptical droplet into a spherical one is dictated by

the ratio of the internal and external viscosities ($\lambda = \eta_{int}/\eta_{ext}$), the radius of the droplet R, and the surface tension σ. [14]

$$\tau = \frac{(2\lambda + 3)(19\lambda + 16)}{40(\lambda + 1)} \frac{\eta_{ext} R}{\sigma} \tag{2}$$

When λ 1 (i.e. η_{int} η_{ext}), the above equation is reduced to equation 1. We calculate τ as the decay time scale of the dimensionless parameter $A \equiv (L-W)/(L+W)$, which is a ratio of the difference and sum of the length (L) and width (W) of a deformed droplet during coalescence (Fig. 1d). Combining those results with measured values of droplet radii and estimated viscosity values obtained from microrheology, surface tensions of NS-liquid droplets in various [NaCl] can be calculated from equation 1.

Conflicts of interest

The authors declare no competing financial interest.

Acknowledgements

Notes and references

1 K. T. Delaney and G. H. Fredrickson, *The Journal of Chemical Physics*, 2017, **146**, 224902.

2 C. G. De Kruif, F. Weinbreck and R. de Vries, *Current opinion in colloid & interface science*, 2004, **9**, 340–349.

3 D. Priftis and M. Tirrell, *Soft Matter*, 2012, **8**, 9396–9405.

4 Z. Xiao, W. Liu, G. Zhu, R. Zhou and Y. Niu, *Journal of the Science of Food and Agriculture*, 2014, **94**, 1482–1494.

5 A. A. Hyman, C. A. Weber and F. Jülicher, *Annual review of cell and developmental biology*, 2014, **30**, 39–58.

6 C. P. Brangwynne, P. Tompa and R. V. Pappu, *Nature Physics*, 2015, **11**, 899–904.

7 F. Smallenburg and F. Sciortino, *Nature Physics*, 2013, **9**, 554.

8 S. Biffi, R. Cerbino, F. Bomboi, E. M. Paraboschi, R. Asselta, F. Sciortino and T. Bellini, *Proceedings of the National Academy of Sciences of the United States of America*, 2013, **110**, 15633–15637.

9 L. Rovigatti, F. Smallenburg, F. Romano and F. Sciortino, *ACS Nano*, 2014, **8**, 3567–3574.

10 D. T. Nguyen and O. A. Saleh, *Soft Matter*, 2017, **13**, 5421–5427.

11 L. L. Josephson, E. M. Furst and W. J. Galush, *Journal of Rheology*, 2016, **60**, 531–540.

12 S. Elbaum-Garfinkle, Y. Kim, K. Szczepaniak, C. C.-H. Chen, C. R. Eckmann, S. Myong and C. P. Brangwynne, *Proceedings of the National Academy of Sciences*, 2015, **112**, 7189–7194.

13 S. Seiffert and W. Oppermann, *Journal of microscopy*, 2005, **220**, 20–30.

14 L. G. Leal, *Advanced Transport Phenomena: Fluid Mechanics and Convective Transport Processes*, Cambridge University Press, Cambridge, 1st edn., 2007.

15 J. SantaLucia, *Proceedings of the National Academy of Sciences*, 1998, **95**, 1460–1465.

16 H. Eyring, *The Journal of Chemical Physics*, 1936, **4**, 283–291.

17 F. Bomboi, S. Biffi, R. Cerbino, T. Bellini, F. Bordi and F. Sciortino, *The European Physical Journal E*, 2015, **38**, 64.

18 J. Fernandez-Castanon, F. Bomboi, L. Rovigatti, M. Zanatta, A. Paciaroni, L. Comez, L. Porcar, C. J. Jafta, G. C. Fadda, T. Bellini and F. Sciortino, *Journal of Chemical Physics*, 2016, **145**, 084910.

19 M. Ortiz-Lombardía, A. González, R. Eritja, J. Aymamí, F. Azorín and M. Coll, *Nature structural biology*, 1999, **6**, 913–917.

20 P. A. Egelstaff, *An introduction to the liquid state*, Clarendon Press, Oxford, 2nd edn., 1994.

21 T. Keyes and I. Oppenheim, *Physical Review A*, 1973, **8**, 937–949.

22 L. Berthier, *Physical Review E*, 2004, **69**, 020201.

23 A. Jaiswal, T. Egami, K. F. Kelton, K. S. Schweizer and Y. Zhang, *Physical Review Letters*, 2016, **117**, 205701.

24 H. Bohidar, P. L. Dubin, P. R. Majhi, C. Tribet and W. Jaeger, *Biomacromolecules*, 2005, **6**, 1573–1585.

25 E. Spruijt, J. Sprakel, M. A. C. Stuart and J. van der Gucht, *Soft Matter*, 2010, **6**, 172–178.

26 E. Spruijt, A. H. Westphal, J. W. Borst, M. A. Cohen Stuart and J. van der Gucht, *Macromolecules*, 2010, **43**, 6476–6484.

27 M. Lemmers, J. Sprakel, I. K. Voets, J. van der Gucht and M. A. C. Stuart, *Angewandte Chemie International Edition*, 2010, **49**, 708–711.

28 D. Priftis, R. Farina and M. Tirrell, *Langmuir*, 2012, **28**, 8721–8729.

29 J. Van der Gucht, E. Spruijt, M. Lemmers and M. A. C. Stuart, *Journal of colloid and interface science*, 2011, **361**, 407–422.

30 E. Spruijt, M. A. C. Stuart and J. van der Gucht, *Macromolecules*, 2013, **46**, 1633–1641.

31 C. P. Brangwynne, C. R. Eckmann, D. S. Courson, A. Rybarska, C. Hoege, J. Gharakhani, F. Jülicher and A. A. Hyman, *Science*, 2009, **324**, 1729–1732.

32 J. Berry, S. C. Weber, N. Vaidya, M. Haataja and C. P. Brangwynne, *Proceedings of the National Academy of Sciences*, 2015, **112**, E5237–E5245.

33 M. Feric, N. Vaidya, T. S. Harmon, D. M. Mitrea, L. Zhu, T. M. Richardson, R. W. Kriwacki, R. V. Pappu and C. P. Brangwynne, *Cell*, 2016, **165**, 1686–1697.

34 M. T. Wei, S. Elbaum-Garfinkle, A. S. Holehouse, C. C. H. Chen, M. Feric, C. B. Arnold, R. D. Priestley, R. V. Pappu and C. P. Brangwynne, *Nature Chemistry*, 2017, **9**, 1118–1125.

35 J.-P. Thiery, G. Macaya and G. Bernardi, *Journal of Molecular Biology*, 1976, **108**, 219–235.

36 S. J. DeCamp, G. S. Redner, A. Baskaran, M. F. Hagan and Z. Dogic, *Nature Materials*, 2015, **14**, 1110–1115.
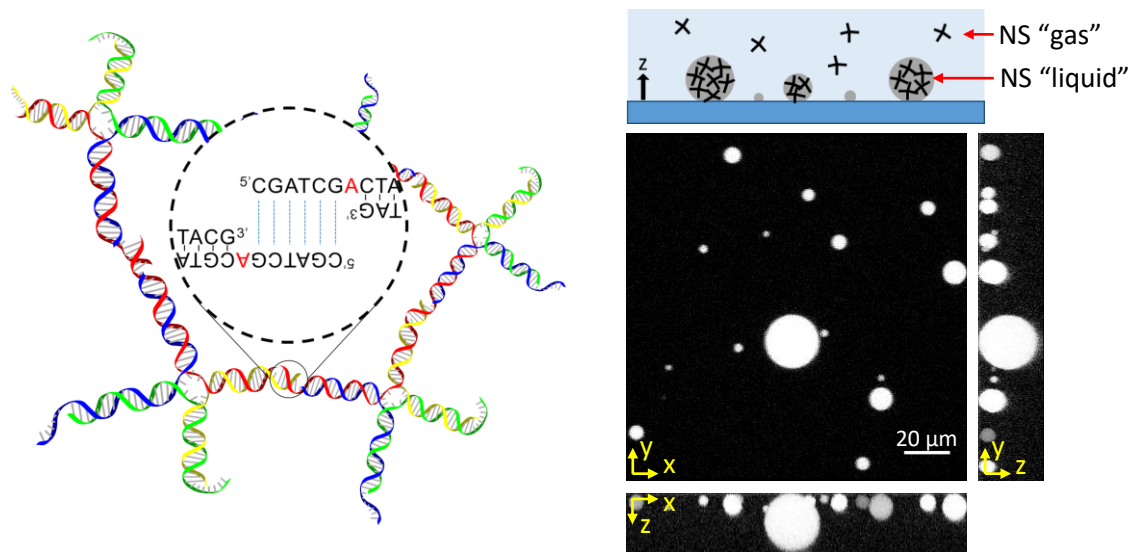
We examine salt-dependent viscosity, self-diffusion, and surface tension of DNA liquid droplets condensed from self-assembled DNA particles ('nanostars') via sticky-end hybridization, showing intriguing characteristics of the DNA liquid, and compare the results to other coacervate systems.